

JENKINS FERROFLUID FLOW LUBRICATION OF A SQUEEZE FILM BETWEEN A SPHERE AND A FLAT POROUS PLATE BASED ON POROSITY AND SLIP VELOCITY

Ramesh Kataria^{*1} & Darshana Patel²

^{*1}Department of Mathematics, M.G. Science Institute, Navrangpura, Ahmadabad, India

²Department of Mathematics and Humanities, Vishwakarma Govt Engineering College, Ahmadabad, India

Abstract:

To investigate the effects of various parameters on ferrofluid lubricated squeeze film bearing with an upper spherical surface and a lower flat porous plate, a mathematical model has been developed. This study examines the effect of slip velocity at the film-porous interface as suggested by Sparrow et al. [1] and modified by Shah et al. [4]. Here, the Jenkins model was used to describe ferrofluid flow behavior. In ferrohydrodynamics, the continuity equation and the equations of the ferrohydrodynamics theory were used to derive a modified Reynolds's type equation governing squeeze film pressure. From the analytical development, expressions for non-dimensional film pressure, load-carrying capacity, and response time using a modified Reynolds-type equation were derived. It was investigated how permeability, minimum film thickness, slip velocity, material constant, and magnetization parameter affect the present mechanism. The results of an investigation indicate that non-dimensional film pressure, load-carrying capacity, and response time decreased with increasing values of the radial permeability parameter, while they increased with increasing values of the axial permeability parameter. In addition, non-dimensional load-carrying capacity increased and response time decreased as minimum film thickness increased. Also, in Jenkins model, non-dimensional load carrying capacity decreased with increasing slip parameter or material parameter values.

MSC 2010: 76S05, 76M25

Keywords: Ferrofluid, Porous plate, Squeeze velocity, Slip velocity, Squeeze film.

DOI: [10.24297/j.cims.2023.7.5](https://doi.org/10.24297/j.cims.2023.7.5)

Nomenclature

a	Radius of the sphere (m)
h	Film thickness defined in Eq. (1) (m)
h_2	Initial film thickness (m)
h_2^*	Non-dimensional initial film thickness as in Eq. (37)
h_m	Minimum film thickness (m)
\dot{h}_m	dh_m / dt , Squeeze velocity ($m s^{-1}$)

h_m^*	Non-dimensional minimum film thickness defined in Eq. (30) (m)
H	Strength of variable magnetic field (Am^{-1})
\mathbf{H}	Magnetic field vector
H_0	Thickness of the porous layer (m)
H^*	Non-dimensional thickness of the porous layer defined in Eq. (30).
K	Defined in Eq. (3) (A^2m^{-4})
\mathbf{M}	Magnetization vector
\mathbf{M}^*	Co-rotational derivative of \mathbf{M}
M_s	Saturation magnetization
M	Magnitude of magnetization vector
p	Film pressure (N m^{-2})
p^*	Non-dimensional film pressure defined in Eq. (30)
\mathbf{q}	Fluid velocity vector, ms^{-1}
r	Radial co-ordinate (m)
R	r/a , non-dimensional radial co-ordinate defined in Eq. (30)
s	Slip parameter defined in Eq. (14) (m^{-1}).
s^*	Non-dimensional slip parameter for p^* and w^* defined in Eq. (30)
s_1^*	Non-dimensional slip parameter for t^* defined in Eq. (37)
t	Time (s)
t^*	Non-dimensional response time as in Eq. (37)
w	Load carrying capacity defined in Eq. (36) (N)
w^*	Non-dimensional load carrying capacity defined in Eq. (36)
z	Axial co-ordinate (m)

Greek symbols

η	Fluid viscosity (N s m^{-2})
η_r	Porosity of the porous region in the radial direction
ρ	Fluid density ($\text{N s}^2 \text{m}^{-4}$)
μ_0	Permeability of free space (N A^{-2})
$\bar{\mu}_0$	Initial susceptibility of fluid
$\bar{\mu}$	Magnetic susceptibility
μ^*	Non-dimensional magnetization parameter for p^* and w^* defined in Eq. (30)
μ_1^*	Non-dimensional magnetization parameter for t^* defined in Eq. (37)
σ	Standard deviation
ϕ_r	Permeability of the fluid in the radial direction of the porous region (m^2)
ϕ_z	Permeability of the fluid in the axial direction of the porous region (m^2)
ϕ_r^*	Non-dimensional radial permeability parameter of the porous region for p^* and w^* is defined by Eq. (30)
ϕ_z^*	Non-dimensional axial permeability parameter of the porous region for p^* and

	W^* defined in Eq. (30)
$\bar{\phi}_r$	Non-dimensional radial permeability parameter of the porous region for t^* defined in Eq. (37)
$\bar{\phi}_z$	Non-dimensional axial permeability parameter of the porous region for t^* defined in Eq. (37)
ψ_r	In Eq. (30), the non-dimensional quantity is defined
ψ_z	In Eq. (30), the non-dimensional quantity is defined
ψ_r^*	Non-dimensional quantity defined in Eq. (37)
ψ_z^*	Non-dimensional quantity defined in Eq. (37)
α^2	Material constant of Jenkins model ($m^3 A^{-1} s^{-1}$)
β^2	Non-dimensional material constant defined in Eq. (30)
γ	another material constant of Jenkins model
γ^*	as defined in Eq. (30)
γ_1^*	as defined in Eq. (37)

1. Introduction

A ferrofluid can be used as a lubricant to eliminate the shortcomings of previous porous bearings studies. Ferrofluid [2] is a colloidal dispersion containing fine ferromagnetic particles, like ferric oxide, cobalt, and magnetite in a non-conducting liquid carrier. A suitable surfactant is added to the carrier liquid to form a coating layer that prevents the particles from flocculating. In the presence of an external magnetic field, magnetic fluid experiences magnetic body forces. In the lack of a magnetic field, the magnetic moments of the particle are randomly oriented and the fluids behave like normal fluids. In a ferrofluid, approximately 85% carrier liquid, 10% surfactant, and 5% magnetic solids are present. When used as a lubricant, ferrofluid has many advantages. There is no rubbing between solid materials, no external lubrication is required, and no side leakage occurs with ferrofluids. These properties make ferrofluids useful for sealing, sensors, filtering devices, elastic dampers, lubrication etc.

Using ferrofluid as a lubricant, Shah and Bhat [3] investigated the lubrication performance of a squeeze film between circular plates with a porous matrix attached to the upper plate using ferrofluid as a lubricant. Consideration of the effect of rotation is also made. Results show that an increase in magnetization parameters increase bearing characteristics such as pressure, load carry capacity, and response time. They also showed that an increase in load-carrying capacity and pressure are entirely dependent on magnetization, while increases in response time depend on fluid inertia, speed of rotation, and magnetization. Under the presence of a ferrofluid, Shah and Kataria [4] studied squeeze film-bearing with a spherical upper surface and a flat porous plate. Their theoretical study investigated the impact of squeeze film height, permeability, and matrix width on squeeze film performance. In their study, the researchers concluded that non-dimensional load-carrying capacity loss due to porosity is almost zero when ferrofluid is used as

a lubricant at smaller values of thickness and radial permeability. The theoretical work on circular discs porous squeeze film bearings of various shapes like exponential, secant, and parallel was done by Shah and Patel [5]. Using the Reynolds equation, different circular porous squeeze film-bearing design systems (e.g., exponential, secant, and parallel (flat)) were studied and compared for load-carrying capacity. According to the findings of the investigation, uniform magnetic fields do not affect the performance of the bearing systems. All the above investigators [3-5] have used the N-R model [6] for ferrofluid lubrication under a variable magnetic field.

Neuringer-Rosensweig (N-R) [6] developed a fairly simple model to examine the effect of magnetic body force, assuming that the magnetization vector \mathbf{M} is parallel to the applied magnetic field vector \mathbf{H} . Jenkins [7] model could be regarded as an extension of the N-R model. The N-R model modifies the pressure while the Jenkins model modifies both the pressure and velocity of the magnetic fluid through an additional term pertaining to the co-rotational derivative of magnetization which is missing in the N-R model. Ram and Verma [8] analyzed the performance of porous inclined slider bearing using Jenkins' ferrofluid flow model [7], which is based on Maugin's [9] simplification of $\mathbf{M} = \mu \mathbf{H}$. Load carrying capacity was found to increase with increasing fluid magnetization and material constant. Shah and Bhat [10] examined the effect of ferrofluid on a slider bearing with a circular convex pad. In their study, researchers indicate that a stronger magnetic field can increase the bearing's pressure and load capacity considerably. However, material parameters do not significantly affect them. Shah and Patel [11] studied the effects of slip and squeeze velocity on a porous pivoted slider bearing lubricated with ferrofluid. In the study, it was found that dimensionless load-carrying capacity increased as squeeze velocity increased and sliding velocity decreased. An extensive review of ferrofluid lubrication with several experimental studies was presented by Huang and Wang [12]. Using the Jenkins model, Laghrabli *et al.* [13] investigated hydrodynamic ferrofluid lubrication for finite journal bearings. The magnetic fluid was generated by displaced finite wire. A comparison was also made between the results and the N-R model. Patel and Kataria [14] presented the Jenkins' model for ferrofluid flow between rotating upper spherical surfaces *and circumferentially rough lower plate, and according to the results, the Jenkins model is more efficient than the NR model at carrying non-dimensional loads. Currently, there is no information on how Jenkins' model impacts the mechanism* [4]. Therefore, further study is of interest to get insight into the phenomenon.

With this motivation, the present study derived a modified Reynolds equation for a ferrofluid lubricated squeeze film bearing consisting of a spherical upper surface and a porous lower surface considering the effects of porosity, squeeze velocity, and slip velocity at the interface of the porous layer and film region using the Jenkins ferrofluid flow model. The validity of Darcy's law is assumed while deriving the modified Reynolds equation. Here, water-based ferrofluid is used. A modified Reynolds's type equation, which is a differential equation in pressure under certain boundary conditions, can be deduced from Navier-Stokes equations along with a continuity equation. Also, equation of continuity is considered in the film as well as the porous

region. From the analytical development, expressions for non-dimensional film pressure and load-carrying capacity of the squeeze film are derived as a function of the non-dimensional parameters such as slip, material constant, magnetization, radial, and axial permeabilities. In this study, the non-dimensional film pressure, load-carrying capacity, and response time were derived and calculated numerically. Graphs depict the results. Table 1 defines the symbols used in the paper. Effects of various non-dimensional parameters like radial permeability, axial permeability, and thickness of porous layer are studied on p^* , W^* , and t^* . Moreover, the effect of minimum film thickness is studied on W^* and t^* . Effect of slip on W^* is illustrated by the graphs.

2. Formulation of the Mathematical Model

As shown in Figure 1, the physical configuration of the problem under consideration is arranged as a rigid sphere with radius a approaching a flat porous plate formed by attaching a layer of porous material of thickness H_0 to an impermeable flat surface. Self-lubrication is one of the advantages of porous layers.

A ferrofluid lubricant fills the region between the sphere and flat porous plate called the fluid film thickness. Film thickness h [4, 14, 15] is given by the expression

$$h = h_m + \frac{r^2}{2a}; \quad r \ll a, \quad (1)$$

where h_m is the minimum film thickness and r is the radial coordinate.

The upper surface (sphere) moves normally towards the lower flat porous plate with a uniform velocity called squeeze velocity

$$\dot{h}_m = \frac{dh_m}{dt}, \quad (2)$$

where t stands for time in seconds.

Strength H of a variable magnetic field [4, 14, 15] is given by

$$H^2 = \frac{Kr^2(a-r)}{a}, \quad (3)$$

K being a quantity chosen to fit the dimensions of both sides of Eq. (3).

2.1 Squeeze film

In 1972, Jenkins developed a simple model to express magnetic fluid flow [7]. Jenkins' theory states that the Neuringer-Rosensweig model was not merely generalized, but also modified in terms of both the pressure and velocity of the magnetic fluid.

According to the Jenkins model, flow equations using the cylindrical frame of reference can be presented as follows [11, 14, 19]:

$$\rho \left[\frac{\partial \mathbf{q}}{\partial t} + (\mathbf{q} \cdot \nabla) \mathbf{q} \right] = -\nabla p + \eta \nabla^2 \mathbf{q} + \mu_0 (\mathbf{M} \cdot \nabla) \mathbf{H} + \rho \alpha^2 \nabla \times \left(\frac{\mathbf{M}}{M} \times \mathbf{M}^* \right), \quad (4)$$

$$\nabla \cdot \mathbf{q} = 0, \quad (5)$$

$$\nabla \times \mathbf{H} = 0, \quad (6)$$

$$\nabla \cdot (\mathbf{H} + 4\pi \mathbf{M}) = 0, \quad (7)$$

$$\gamma \frac{D^2 \mathbf{M}}{Dt^2} = -4\pi \rho \frac{M_s}{\mu_0} \frac{\mathbf{M}}{(M_s - M)} - \frac{2\alpha^2}{M} \mathbf{M}^* + \mathbf{H}, \quad (8)$$

$$\mathbf{M}^* = \frac{D\mathbf{M}}{Dt} + \frac{1}{2} (\nabla \times \mathbf{q}) \times \mathbf{M}. \quad (9)$$

In the present analysis, the direction of the magnetization of a fluid is always in the direction of the local magnetic field [11, 14, 18], so Eq. (9) is replaced by

$$\mathbf{M} = \bar{\mu} \mathbf{H}, \quad (10)$$

and
$$\mathbf{M}^* = \frac{1}{2} (\nabla \times \mathbf{q}) \times \mathbf{M}, \quad (11)$$

Also,
$$\mathbf{q} = (\dot{r}, r\dot{\theta}, \dot{z}) = (u, rv, w), \quad (12)$$

where (r, θ, z) are cylindrical polar co-ordinates and dot ($\dot{\cdot}$) represents derivative with respect to t . Also, a radial, tangential, and axial velocity component of \mathbf{q} is given by u, v , and w .

For the derivation, laminar flow and fluid incompressibility are assumed, porous matrix is homogeneous and isotropic, all inertia terms are neglected because viscous forces are greater than inertia forces. Flow within the film and porous region are axisymmetric, derivatives of fluid velocities across the film predominate, and velocities are continuous at the interface between the porous layer and film regions.

Based on the simplified assumptions and using Eqs. (4) to (9), a two-dimensional equation governing the distribution of pressure p in the r -direction is given by [11, 19]. (Appendix B)

$$\frac{\partial}{\partial z} \left(\eta \frac{\partial u}{\partial z} \right) = \frac{1}{\left(1 - \frac{\rho \alpha^2 \bar{\mu} H}{2\eta} \right)} \frac{\partial}{\partial r} \left(p - \frac{1}{2} \mu_0 \bar{\mu} H^2 \right), \quad (13)$$

where H is the magnetic field strength. By solving Eq. (13) under the boundary conditions [1, 4, 23]

$$u = \frac{1}{s} \frac{\partial u}{\partial z}, \text{ when } z = 0; \frac{1}{s} = \frac{\sqrt{\phi_r \eta_r}}{5} \text{ (slip boundary condition)} \quad (14)$$

And $u = 0$, when $z = h$, (15)

we obtain a velocity profile along the film region as follows (Appendix A)

$$u = \left\{ \frac{(h+z+shz)(z-h)}{2\eta(1+sh)\left(1-\frac{\rho\alpha^2\bar{\mu}H}{2\eta}\right)} \right\} \frac{\partial}{\partial r} \left(p - \frac{1}{2} \mu_0 \bar{\mu} H^2 \right), \quad (16)$$

where s : slip parameter, ϕ_r : permeability of the porous region in the radial direction, η_r : porosity of the porous region in the radial direction.

Eq. (16) is integrated over the film region h , i.e., 0 to h , with respect to z , we obtain

$$\int_0^h u \, dz = \left\{ \frac{h^3 (4 + sh)}{12\eta (1 + sh) \left(1 - \frac{\rho\alpha^2 \bar{\mu} H}{2\eta} \right)} \right\} \frac{\partial}{\partial r} \left(P - \frac{1}{2} \mu_0 \bar{\mu} H^2 \right). \quad (17)$$

Using continuity equation in cylindrical polar coordinates and integrating it with respect to z over the film thickness $[0, h]$ yields

$$\frac{1}{r} \frac{\partial}{\partial r} \int_0^h (ru) \, dz + w_h - w_0 = 0. \quad (18)$$

Taking Eq. (17) into account, Eq. (18) becomes

$$w_0 = \dot{h}_m - \frac{1}{r} \frac{\partial}{\partial r} \left[\frac{r h^3 (4 + sh)}{12\eta (1 + sh) \left(1 - \frac{\rho\alpha^2 \bar{\mu} H}{2\eta} \right)} \frac{d}{dr} \left(P - \frac{1}{2} \mu_0 \bar{\mu} H^2 \right) \right], \quad (19)$$

where $w_h = w|_{z=h} = \dot{h}_m$ which represents the effect of squeeze velocity in the z - direction.

Also,

$$w|_{z=0} = w_0. \quad (20)$$

The pressure distribution $p = p(r)$, which appears in Eqs. (16), (17), and (19), is not considered a priori. Our aim is to determine pressure distribution $p = p(r)$ as a key to the solution of the problem. To find pressure distribution $p(r)$, it is necessary to examine the flow process in the porous layer and to employ conditions of continuity at the interface of porous layer and film region.

2.2 Porous medium

In the porous layer, the velocity components \bar{u} and \bar{w} are related to the pressure P by Darcy's law. The components of radial and axial velocity of the fluid in the porous region are given as [23]

$$\bar{u} = \frac{-\phi_r}{\eta} \left[\frac{\partial}{\partial r} \left(P - \frac{1}{2} \mu_0 \bar{\mu} H^2 \right) + \frac{\rho\alpha^2 \bar{\mu}}{2} \frac{\partial}{\partial z} \left(H \frac{\partial u}{\partial z} \right) \right] \text{ and} \quad (21)$$

$$\bar{w} = \frac{-\phi_z}{\eta} \left[\frac{\partial}{\partial z} \left(P - \frac{1}{2} \mu_0 \bar{\mu} H^2 \right) - \frac{\rho\alpha^2 \bar{\mu}}{2r} \frac{\partial}{\partial r} \left(rH \frac{\partial u}{\partial z} \right) \right], \quad (22)$$

where ϕ_r, ϕ_z represents the radial and axial permeability of the fluid in the porous region. Also, P indicates fluid pressure of porous region.

In the porous layer, continuity equation can be expressed as follows [23]

$$\frac{1}{r} \frac{\partial}{\partial r} (r\bar{u}) + \frac{\partial \bar{w}}{\partial z} = 0, \quad (23)$$

substituting Eqs. (21) and (22) in Eq. (23), and integrating over the thickness of the porous layer H_0 that is, over the interval $(-H_0, 0)$ yields

$$-\phi_z \frac{\partial}{\partial z} \left(p - \frac{1}{2} \mu_0 \bar{\mu} H^2 \right) \Big|_{z=0} = \frac{\phi_r H_0}{r} \frac{\partial}{\partial r} \left[r \frac{\partial}{\partial r} \left(p - \frac{1}{2} \mu_0 \bar{\mu} H^2 \right) \right] + \frac{\rho \alpha^2 \bar{\mu}}{2} (\phi_r - \phi_z) \frac{1}{r} \frac{\partial}{\partial r} \left(r H \frac{\partial u}{\partial z} \right) \Big|_{z=-H_0} \quad (24)$$

2.3 Continuity conditions

Based on the Morgan-Cameron [4, 18] approximations continuity of pressure

$$\frac{\partial}{\partial r} \left(p - \frac{1}{2} \mu_0 \bar{\mu} H^2 \right) = \frac{\partial}{\partial r} \left(p - \frac{1}{2} \mu_0 \bar{\mu} H^2 \right), \quad (25)$$

when employing to Eq. (24) takes the form

$$\frac{\partial}{\partial z} \left(p - \frac{1}{2} \mu_0 \bar{\mu} H^2 \right) \Big|_{z=0} = -\frac{\phi_r H_0}{r \phi_z} \frac{\partial}{\partial r} \left[r \frac{\partial}{\partial r} \left(p - \frac{1}{2} \mu_0 \bar{\mu} H^2 \right) \right] - \frac{\rho \alpha^2 \bar{\mu}}{2 \phi_z} (\phi_r - \phi_z) \frac{1}{r} \frac{\partial}{\partial r} \left(r H \frac{\partial u}{\partial z} \right) \Big|_{z=-H_0} \quad (26)$$

Using Eqs. (22), (25), and (26), we have

$$\bar{w}_0 = \frac{1}{r} \frac{\partial}{\partial r} \left[\left\{ \frac{\phi_r H_0}{\eta} + \frac{\rho \alpha^2 \bar{\mu} (\phi_r - \phi_z) H H_0}{2 \eta^2 \left(1 - \frac{\rho \alpha^2 \bar{\mu} H}{2 \eta} \right)} - \frac{\rho \alpha^2 \bar{\mu} \phi_z H s h^2}{4 \eta^2 (1 + s h) \left(1 - \frac{\rho \alpha^2 \bar{\mu} H}{2 \eta} \right)} \right\} r \frac{\partial}{\partial r} \left(p - \frac{1}{2} \mu_0 \bar{\mu} H^2 \right) \right] \quad (27)$$

The normal (axial) component of the fluid velocity at the film-porous interface at the lower disc is assumed to be continuous, that is [11],

$$w_0 = \bar{w}_0 \quad (28)$$

Produces the Reynolds' type equation as follows

$$\frac{1}{r} \frac{\partial}{\partial r} \left[\left\{ 12 \phi_r H_0 + \frac{\eta h^3 (4 + s h) - 3 \rho \alpha^2 \bar{\mu} \phi_z s h^2 H}{\eta (1 + s h) \left(1 - \frac{\rho \alpha^2 \bar{\mu} H}{2 \eta} \right)} + \frac{6 \rho \alpha^2 \bar{\mu} H_0 (\phi_r - \phi_z) H}{\eta \left(1 - \frac{\rho \alpha^2 \bar{\mu} H}{2 \eta} \right)} \right\} r \frac{\partial}{\partial r} \left(p - \frac{1}{2} \mu_0 \bar{\mu} H^2 \right) \right] = 12 \eta \dot{h}_m, \quad (29)$$

for the considered phenomenon.

Introduce the following non-dimensional variables as

$$R = \frac{r}{a}, \quad h_m^* = \frac{h_m}{a}, \quad h^* = \left(\frac{a h}{h_m^2} \right) h_m^*, \quad \phi_r^* = \frac{\phi_r a}{h_m^3}, \quad p^* = -\frac{p h_m^3}{a^2 \eta \dot{h}_m}, \quad \gamma^* = \frac{6 \phi_z}{h_m^2}, \quad \beta^2 = \frac{\rho \alpha^2 \bar{\mu} \sqrt{k} a}{2 \eta},$$

$$H^* = \frac{H_0}{a}, \quad \phi_z^* = \frac{\phi_z a}{h_m^3}, \quad \psi_r = \phi_r^* H^*, \quad s^* = s h_m, \quad \mu^* = -\frac{K \mu_0 \bar{\mu} h_m^3}{\eta \dot{h}_m}, \quad \psi_z = \phi_z^* H^*. \quad (30)$$

Eq. (29) can be expressed non-dimensionally as follows

$$\frac{d}{dR} \left[G R \frac{d}{dR} \left\{ p^* - \frac{1}{2} \mu^* R^2 (1 - R) \right\} \right] = -12 R, \quad (31)$$

where

$$G = 12 \psi_r + \frac{h^{*3} (4 + s^* h^*)}{(1 + s^* h^*) (1 - \beta^2 R \sqrt{1 - R})} - \frac{\beta^2 \gamma^* s^* h^{*2} R \sqrt{1 - R}}{(1 + s^* h^*) (1 - \beta^2 R \sqrt{1 - R})} + \frac{12 \beta^2 (\psi_r - \psi_z) R \sqrt{1 - R}}{(1 - \beta^2 R \sqrt{1 - R})}.$$

The non-dimensional thickness of the film is calculated as follows:

$$h^* = 1 + \frac{R^2}{2h_m^*}. \quad (32)$$

Further, non-dimensional form of the magnetic field H defined in Eq. (3) is

$$H^2 = K\alpha^2 R^2 (1 - R). \quad (33)$$

3. Solutions

Applying pressure boundary conditions [4]

$$p^* = 0 \text{ at } R = 1$$

(Since, the atmospheric pressure is negligible compared to the film pressure)

$$\text{and } \frac{\partial p^*}{\partial R} = 0 \text{ at } R = 0$$

(34)

to Eq. (31), the non-dimensional film pressure p^* can be derived as follows

$$p^* = \frac{1}{2} \mu^* R^2 (1 - R) + \int_R^1 \frac{6R}{G} dR \quad (35)$$

where

$$G = 12\psi_r + \frac{h^{*3}(4 + s^*h^*)}{(1 + s^*h^*)(1 - \beta^2 R\sqrt{1 - R})} - \frac{\beta^2 \gamma^* s^* h^{*2} R\sqrt{1 - R}}{(1 + s^*h^*)(1 - \beta^2 R\sqrt{1 - R})} + \frac{12\beta^2(\psi_r - \psi_z)R\sqrt{1 - R}}{(1 - \beta^2 R\sqrt{1 - R})}.$$

And the non-dimensional load carrying capacity W^* can be derived as follows [4]

$$W^* = \frac{-Wh_m^3}{2\pi\eta a^4 h_m} = \frac{\mu^*}{40} + 3 \int_0^1 \frac{R^3}{G} dR. \quad (36)$$

Again, introducing non-dimensional quantities for calculating response time t as

$$h_2^* = \frac{h_m}{h_2}, \mu_1^* = \frac{K\mu_o \bar{\mu} a^4}{W}, \bar{\phi}_r = \frac{\phi_r a}{h_2^3}, \bar{\phi}_z = \frac{\phi_z a}{h_2^3}, \psi_r^* = \bar{\phi}_r H^*, \psi_z^* = \bar{\phi}_z H^*, t^* = \frac{h_2^2 W t}{\eta a^4}, s_1^* = s h_2, \gamma_1^* = \frac{6\bar{\phi}_z}{h_2^2}. \quad (37)$$

Using Eq. (37), the non-dimensional response time t^* to reach a film thickness starting with an initial film thickness h_2 is given by

$$t^* = - \int_{h_2^*}^1 \frac{\int_0^1 \frac{3R^3}{G^*} dR}{\left(-\frac{1}{2\pi} + \frac{\mu_1^*}{40}\right)} dh_2^*, \quad (38)$$

where

$$G = \frac{G^*}{h_2^{*3}}, G^* = 12\psi_r^* + \frac{(h_2^*)^3 h_m^{*3} (4 + s_1^* h_2^* h_m^*)}{(1 + s_1^* h_2^* h_m^*)(1 - \beta^2 R\sqrt{1 - R})} - \frac{\beta^2 h_2^{*2} \gamma_1^* s_1^* h_m^{*3} R\sqrt{1 - R}}{(1 + s_1^* h_2^* h_m^*)(1 - \beta^2 R\sqrt{1 - R})} + \frac{12\beta^2 R\sqrt{1 - R}(\psi_r^* - \psi_z^*)}{(1 - \beta^2 R\sqrt{1 - R})}. \quad (39)$$

4. Discussion of Results

This study analyzes squeeze film characteristics between an upper sphere and a flat porous plate using ferrofluid as a lubricant in the presence of an oblique and variable magnetic field. Here, ferrofluid lubricant flowing as per the Jenkins model simplified by Maugin [9] and used by Ram and Verma [8]. The modified Reynolds-Darcy equation is derived. In this paper, the effects of non-dimensional radial permeability, axial permeability, and the thickness of porous matrix are studied on the non-dimensional film pressure and response time. Eqs. (35), (36) and (38) show non-dimensional pressure distribution p^* , load carrying capacity w^* and response time t^* . A numerical evaluation of these parameters could be made using Simpson's one-third rule by dividing the interval into subintervals to see how various parameters affect.

The following values are taken into account in all computations.

$W = 25.0 \text{ N}$, $\eta = 0.012 \text{ (Nsm}^{-2}\text{)}$, $\eta_r = 0.25$, $\bar{\mu} = 0.05$, $H_0 = 0.001$, $\mu_0 = 4\pi \times 10^{-7} \text{ (NA}^{-2}\text{)}$,
 $\dot{h}_m = -0.04 \text{ (ms}^{-1}\text{)}$, $K = 10^9 / 1.48 \text{ (A}^2 / \text{m}^4\text{)}$, $a = 0.01 \text{ (m)}$, $r = 0.0001 \text{ (m)}$, $\beta^2 = 0.5$
 $h_m = 0.00008 \text{ (m)}$ (Fixed for Figs. 2, 3, 4, 5, 6, 9, 10, and 11), $h_m = 0.00001 \text{ (m)}$ (For Fig. 8)
 $\phi_z = 10^{-16} \text{ (m}^2\text{)}$ (Fixed for Figs. 6, 7, 8, 9, and 12), $\phi_r = 10^{-16} \text{ (m}^2\text{)}$ (For Fig. 8), $\phi_r = 10^{-11} \text{ (m}^2\text{)}$
(Fixed for Figs. 3, 4, 5, 7, 9, 10, and 12), $H_0 = 0.001$ (Fixed for Figs. 2, 4, 5, 6, 8, 10, and 11),
 $H_0 = 0.00001$ (For Fig. 9). $H_0 = 0.0000001$ (For Fig. 7).

In Chan and Horn [20] analyzed the Reynolds lubrication equation for a sphere moving normal towards a flat surface at a separation h_0 . As a result of their study, they also found that the equation

$$\frac{1}{r} \frac{d}{dr} \left[r h_n^3(r) \frac{d}{dr} (p(r)) \right] = 12 \eta \dot{h}_m' \quad (40)$$

holds for spherical surfaces for the pressure distribution $p(r)$. Here at radius r , $h_n(r)$ is the surface separation. $h_n(r)$ can be expressed mathematically as $h_n = h_m + \frac{r^2}{2a}$,

where $r \ll R$, h_m is the nominal smooth part of the surface and r is the radial coordinate.

Matthewson [21] used Eq. (40) to derive an analytical equation for the squeeze flow of Newtonian fluid between a smooth rigid sphere and a smooth rigid flat plate to describe liquid flow in a liquid bridge. The squeeze film between a sphere and a flat plate was theoretically studied by Lin *et al.* [22]. As a result, they have derived the Reynolds equation for calculating pressure distributions in the form

$$\frac{1}{r} \frac{\partial}{\partial r} \left[\left\{ h^3 - 12l^2 h + 24l^3 \tanh \left(\frac{h}{2l} \right) \right\} r \frac{dp}{dr} \right] = 12 \eta \dot{h} \quad (41)$$

where l is the characteristics length of the additives responsible for the couple-stress effect and h is given by Eq. (1). When a Newtonian fluid is used, Eq. (41) becomes Eq. (40).

By using the Neuringer-Rosensweig (N-R) model, Shah and Kataria [4] studied ferrofluid lubricated squeeze film action between an upper sphere and a lower flat porous plate. This work is an extension of the work presented by Chan and Horn [20] and Lin *et al.* [22] in the realm of Reynolds equations for pressure distribution and porous layer insertion with lower plates. They also considered ferrofluid as a lubricant with a variable and oblique magnetic field rather than conventional as well as couple-stress fluids. Present research paper extends the work of Shah and Kataria [4] in terms of ferrofluid flow behavior described by Jenkins model instead of Neuringer-Rosensweig (N-R). In their paper, Shah and Kataria [4] ignore the term pertaining to the co-rotational derivative of magnetization. As a result, this gap has been filled in the present study.

4.1 Discussion on squeeze film pressure

Figure 2 shows the non-dimensional film pressure p^* as a function of non-dimensional radial permeability parameter of the porous region ϕ_r^* for different values of axial permeability parameter ϕ_z^* keeping non-dimensional minimum film height $h_m^* = 0.008$. It is seen that p^* almost remains same when $1.95 \times 10^{-6} \leq \phi_r^* \leq 1.95 \times 10^{-3}$. However, for $\phi_r^* > 1.95 \times 10^{-3}$, p^* decreases. It is observed, in general, that p^* increases with the increasing values of ϕ_z^* .

The variation in non-dimensional film pressure p^* as a function of non-dimensional thickness of porous matrix H^* for different values of axial permeability parameter ϕ_z^* keeping non-dimensional minimum film height $h_m^* = 0.008$ is shown in figure 3. It is shown that when $0 \leq H^* < 0.01$, p^* attains almost same value. For $H^* \geq 0.01$, p^* starts decreasing. As a result, the insertion of porous layer reduces load carrying capacity and ultimately pressure which supports the conclusion of [1, 16, 18] Also, it is observed that p^* increases with the increasing values of ϕ_z^* .

Figure 4 shows the non-dimensional film pressure p^* as a function of non-dimensional axial permeability parameter of the porous region ϕ_z^* at non-dimensional minimum film height $h_m^* = 0.008$. It is observed that p^* almost remains same when $1.95 \times 10^{-6} \leq \phi_z^* \leq 1.95 \times 10^{-3}$. However, for $\phi_z^* > 1.95 \times 10^{-3}$, p^* increases. From figures 2, 3 and 4, p^* attains maximum value when $1.95 \times 10^{-6} \leq \phi_r^* \leq 1.95 \times 10^{-3}$, $0 \leq H^* < 0.01$, and $\phi_z^* > 1.95 \times 10^{-3}$.

4.2 Discussion on load carrying capacity

Figure 5 shows the non-dimensional load carrying capacity w^* as a function of non-dimensional axial permeability parameter of the porous region ϕ_z^* at fixed parametric value $h_m^* = 0.008$. It is observed from the figure that initially for $1.95 \times 10^{-6} \leq \phi_z^* \leq 1.95 \times 10^{-3}$, there is no variation in w^* but there after w^* increases with the increase of ϕ_z^* .

Figure 6 shows the variation in non-dimensional load carrying capacity w^* as a function of the non-dimensional radial permeability parameter of the porous region ϕ_r^* at non-dimensional

minimum film thickness $h_m^* = 0.008$. It is observed that the variation in w^* remains almost same when $1.95 \times 10^{-6} \leq \phi_r^* \leq 1.95 \times 10^{-3}$. But $\phi_r^* > 1.95 \times 10^{-3}$, w^* decreases.

In Figure 7, the non-dimensional load carrying capacity w^* is plotted against the non-dimensional minimum film thickness h_m^* with varying non-dimensional thickness of porous matrix H^* at $\phi_z^* = 1.95 \times 10^{-6}$. It is observed that with increasing h_m^* , w^* increases. For $H^* = 0.00001$, a higher load carrying capacity w^* can be achieved. Also, w^* reaches nearly the same value when $0.005 \leq h_m^* \leq 0.009$ and $0.00001 \leq H^* \leq 0.01$. After $H^* = 0.0001$, w^* starts decreasing for $0.001 \leq h_m^* \leq 0.004$, whereas before that it is constant. Shah *et al.* [4] reported the same behavior.

Figure 8 shows the non-dimensional load carrying capacity w^* as a function of non-dimensional material constant β^2 for various values of $1/s^*$ at fixed parametric value $\phi_r^* = 1.95 \times 10^{-6}$ and $h_m^* = 0.001$. It is observed that w^* decreases when material constant β^2 increases. The effect of material constant parameter modifies the velocity of the ferrofluid which leads to decreased pressure resulting in reduced load carrying capacity. The observation of Shah *et al.* [18] in agreement with these findings. Also, w^* increases when $1/s^*$ decreases. It may be that slip reduces the resistance encountered by fluid flowing through the gap, thus lowering its load-carrying capacity. This is in agreement with the theoretical findings of Sparrow *et al.* [1], as well as Shah *et al.* [18].

Figure 9 shows the non-dimensional load carrying capacity w^* as a function of non-dimensional magnetization parameter μ^* (where K varies) considering $H^* = 0.001$. It is observed that w^* increases moderately with the increasing values of μ^* up to 4.53×10^{-2} , but beyond that it increases. It may be caused by higher magnetic fields causing stronger ferrofluid spikes to form. The magnetization induces an increase in the viscosity of the lubricant which leads to increased pressure and therefore to the increased load carrying capacity.

4.3 Discussion on squeeze film time

Figure 10 presents the non-dimensional response time t^* as a function of non-dimensional axial permeability parameter of the porous region $\bar{\phi}_z$ at non-dimensional minimum film thickness $h_m^* = 0.008$. It is seen that for $1.95 \times 10^{-6} \leq \bar{\phi}_z \leq 1.95 \times 10^{-2}$ there is no variation in t^* . Also, for $\bar{\phi}_z > 1.95 \times 10^{-2}$, t^* increases.

Figure 11 shows the non-dimensional response time t^* as a function of non-dimensional radial permeability parameter of the porous region $\bar{\phi}_r$ for different values of axial permeability parameter $\bar{\phi}_z$. It is observed that for $1.95 \times 10^{-6} \leq \bar{\phi}_r \leq 1.95 \times 10^{-3}$, t^* remains constant. However, for $\bar{\phi}_r > 1.95 \times 10^{-3}$, t^* decreases. It is observed, in general, that t^* increases with the increasing values of $\bar{\phi}_z$.

Figure 12 presents the non-dimensional response time t^* as a function of non-dimensional thickness of porous matrix H^* for different values of non-dimensional minimum film thickness h_m^* . It is observed that t^* decreases as h_m^* increases. When $0.005 \leq h_m^* \leq 0.009$ and $0.00001 \leq H^* \leq 0.01$, t^* attains almost the same value. For $0.001 \leq h_m^* \leq 0.004$, t^* starts decreasing after $H^* = 0.0001$ whereas before that it takes constant value.

The present analysis reduces to the case of Shah *et al.* [4] by setting $\alpha^2 = 0$. The case will further deduce to Shah *et al.*[15], when there is no porous matrix attached to lower plate and surface roughness effect and rotation effect at both (upper and lower) surfaces in addition. The present analysis reduces to the no slip case by setting $\frac{1}{s^*} \rightarrow 0$. The present case reduces to the case of conventional lubricant when $\mu^* = 0$.

5. Conclusion

By using Jenkins model, flow was described for a ferrofluid-lubricated squeeze film bearing composed of a sphere on top and a flat base on the bottom. Here, a porous facing is attached with a lower plate. The modified Reynolds equation, governing the squeeze film pressure, is derived by considering the effects of squeeze velocity and slip velocity. The validity of the Darcy's law is assumed for the porous matrix. Due to its significant impact on bearing characteristics, the co-rotational derivative of magnetization has also been taken into account which Shah and Kataria ignored in[4]. The expression for non-dimensional load carrying capacity W^* is obtained from the pressure equation. The effects of non-dimensional radial permeability parameter, axial permeability parameter, and thickness of porous matrix are studied on p^* , W^* and t^* whereas effects of non-dimensional magnetization parameter and slip parameter are studied on w^* . We also investigate the effect of minimum film thickness on w^* and t^* . The non-dimensional film pressure, load carrying capacity, and response time decreased as the radial permeability parameter increased, but they increased as the axial permeability parameter increased. The non-dimensional response time decreases and non-dimensional load carrying capacity increases with increasing minimum film thickness values. Furthermore, the material constant of Jenkins model also caused the non-dimensional load carrying capacity to decrease. In addition, Jenkins model may also be adopted when slip is minimum.

The results of the present study led to the following conclusions:

Non-dimensional film pressure p^* remains maximum and constant, when

- (i) $1.95 \times 10^{-6} \leq \phi_r^* \leq 1.95 \times 10^{-3}$.
- (ii) when $0 < H^* < 0.01$. And p^* increases with the increasing values of ϕ_z^* .

Non-dimensional load carrying capacity w^*

- (i) decreases as β^2 moves from 0.02 to 1.6.

- (ii) decreases as $\frac{1}{s^*}$ increases. And increases with the increasing values of non dimensional magnetization parameter μ^* and the increase rate is more with the generation of stronger spikes of the ferrofluid due to higher magnetic field.

The nature of non-dimensional response time t^* attains maximum for $h_m^* = 0.001$, $H^* = 0.00001$ and $1.95 \times 10^{-6} \leq \bar{\phi}_r \leq 1.95 \times 10^{-3}$ remains almost constant for $0.005 \leq h_m^* \leq 0.009$, $0.00001 \leq H^* \leq 0.01$. increases with the increasing values of $\bar{\phi}_z$.

The pressure in the porous medium creates a path for fluid to flow from the bearing into the environment, which is different from permeability, according to Sparrow *et al.* [1]. Generally speaking, the higher the permeability, the faster fluid flows through the porous material. As a result, the porous material reduces resistance to flow in the r -direction, which consequently reduces load-carrying capacity. A similar tendency to decrease load-carrying capacity with the introduction of porous matrix and high permeability is also observed by Prakash and Tiwari [16], as well as by Wu [17].

In our case, porosity reduces loss of w^* almost to zero. It is due to the use of ferrofluid as a lubricant, it is controlled by an oblique, variable magnetic field for smaller values of H^* and $\bar{\phi}_r^*$.

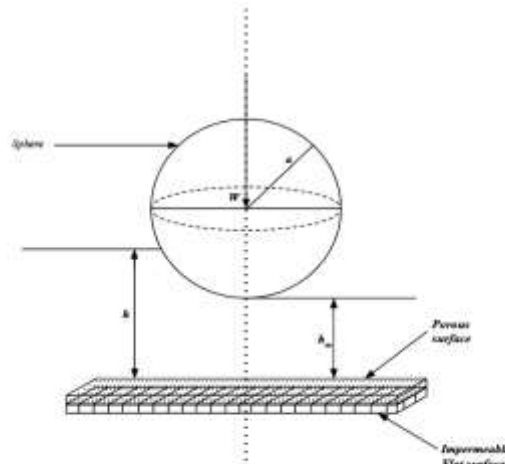


Fig.1 Squeeze film geometry between a sphere and a flat porous plate

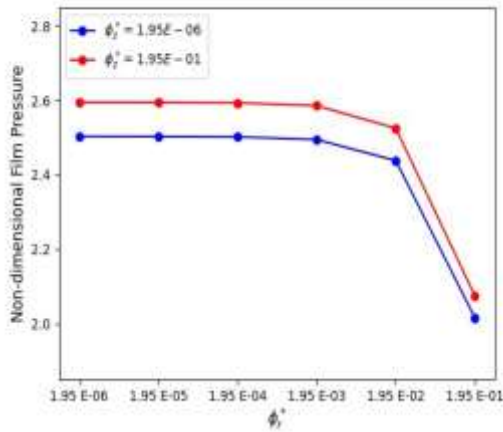


Fig. 2 p^* versus ϕ_r^* for different values of ϕ_z^*

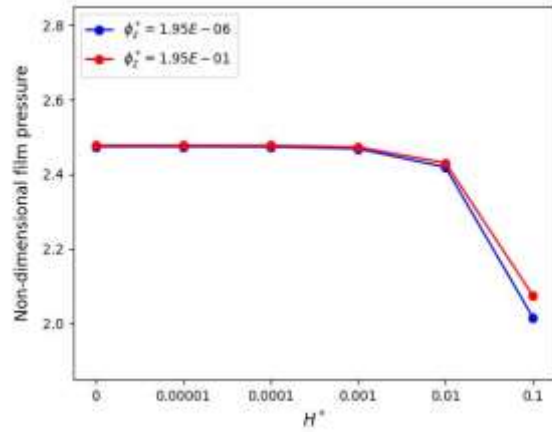


Fig. 3 p^* versus H^* for different values of ϕ_z^*

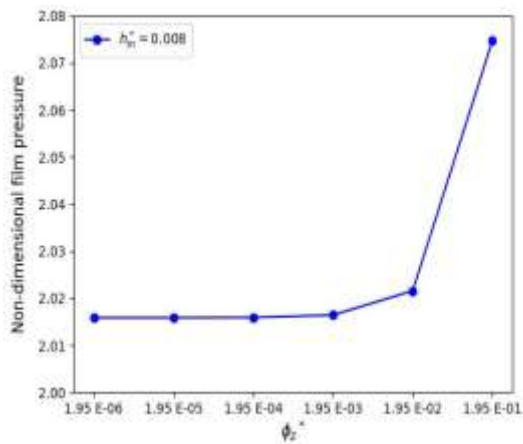


Fig. 4 p^* versus ϕ_z^* at $h_m^* = 0.008$

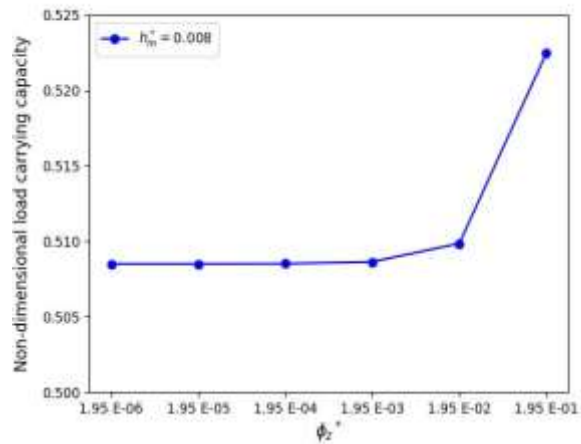


Fig. 5 W^* versus ϕ_z^* at $h_m^* = 0.008$

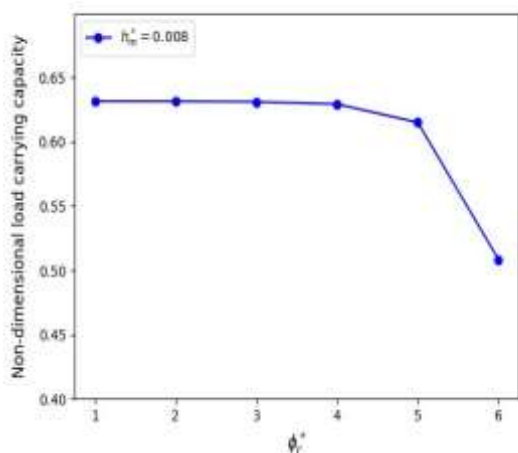


Fig. 6 W^* versus region ϕ_r^* at $h_m^* = 0.008$

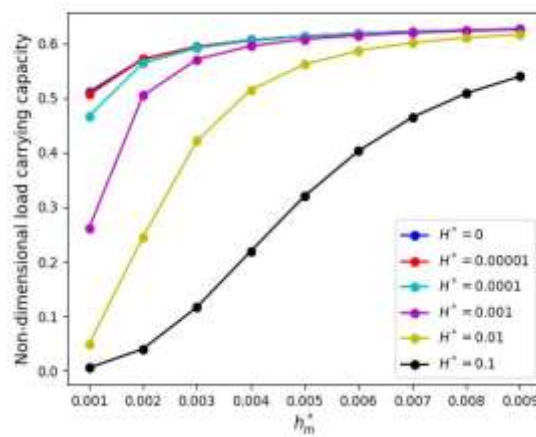


Fig. 7 W^* versus h_m^* for different values of H^*

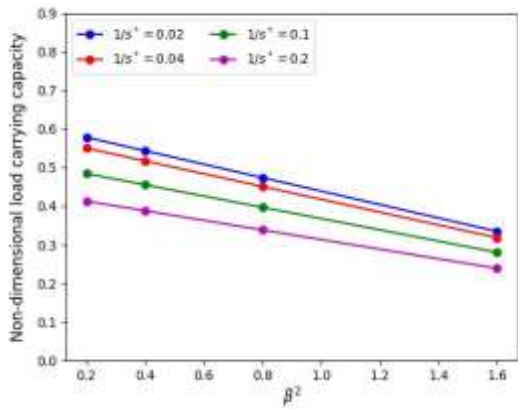


Fig. 8 W^* versus β^2 for various values of $1/s^*$

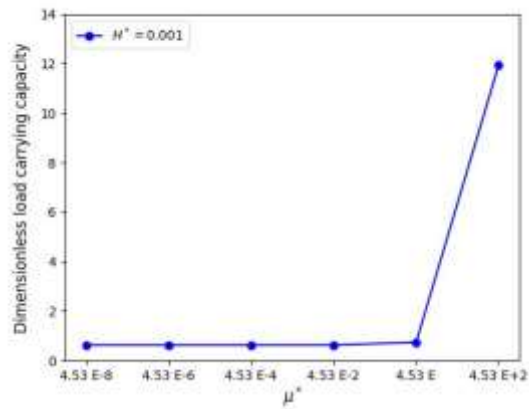


Fig. 9 W^* versus μ^* for $H^* = 0.001$

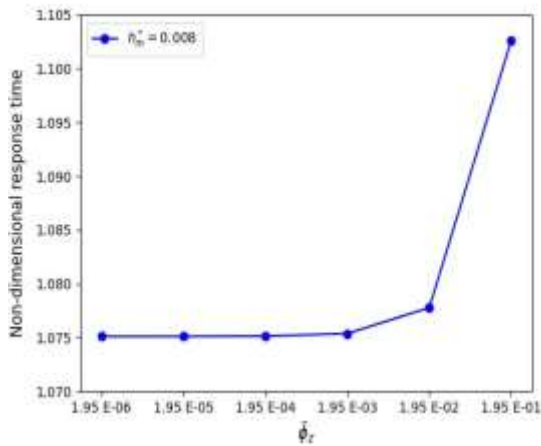


Fig. 10 t^* versus $\bar{\phi}_z$ at $h_m^* = 0.008$

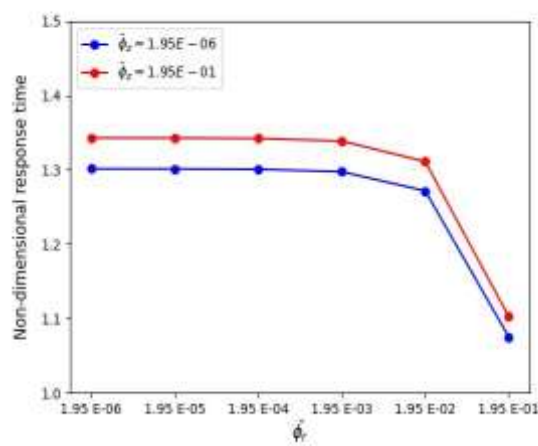


Fig. 11 t^* versus $\bar{\phi}_r$ for different values $\bar{\phi}_z$

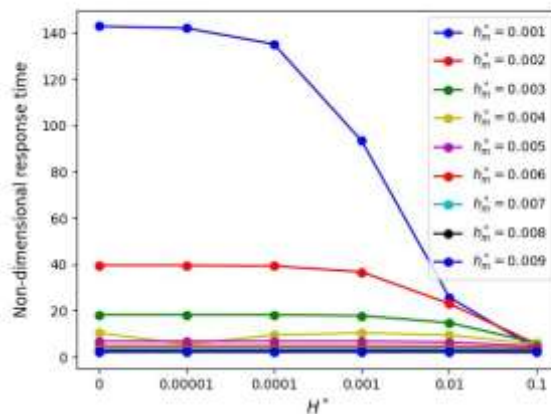


Fig. 12 t^* versus H^* for different values of h_m^* .

References

1. Sparrow, E. M., Beavers, G. S., & Hwang, I. T. (1972). Effect of velocity slip on porous walled squeeze films. *Journal of lubrication Technology*, 94(3), 260-265.
2. Rosensweig, R. E. (1985). *Ferrohydrodynamics*. Cambridge University Press.

3. Shah, R.C., & Bhat, M.V. (2000). Squeeze film based on magnetic fluid in curved porous rotating circular plates. *Journal of Magnetism and Magnetic Materials*, 208:115–119.
4. Shah, R.C. & Kataria, R.C. (2016). On the squeeze film characteristics between a sphere and a flat porous plate using ferrofluid. *Applied Mathematical Modeling*, Volume 40, 2473-2484.
5. Shah, R.C., & Patel, D. B. (2017). Analysis and comparative study of ferrofluid lubricated circular porous squeeze film-bearings. *Journal of Engineering Tribology*, 231(11), 1450-1463.
6. Neuringer, J. L., & Rosensweig, R.E. (1964). Ferrohydrodynamics. *The Physics of Fluids*, 7:1927-1937.
7. Jenkins, J.T. (1972). A theory of magnetic fluids. *The Archive of Rational Mechanics and Analysis*, 46(1), 42-60.
8. Paras, R., & Verma, P.D.S. (1999). Ferrofluid lubrication in porous inclined slider bearing. *Indian Journal of Pure Applied Mathematics*, 30 (12): 1273-1281.
9. Maugin, G. A. (1980). The method of virtual power in continuum mechanics: Application to coupled fields. *Acta Mechanica*, 35(1-2): 1-70.
10. Shah, R.C., & Bhat, M.V. (2004). Ferrofluid lubrication of a slider bearing with a circular convex pad. *Journal of National Science Foundation of Sri Lanka*, 32(3-4):139-148.
11. Shah, R.C., & Patel, D. B. (2014). Magnetic fluid lubrication of porous pivoted slider bearing with slip and squeeze velocity. *International Journal of Industrial Mathematics*, 6(3), 199-206.
12. Huang, W., & Wang, X. (2016). Ferrofluids lubrication: A status report. *Lubrication Science*, 28, 3-26.
13. Laghrabli, S., Khelifi, M. El., Nabhani, M., & Bou-saïd, B. (2017). Ferrofluid Lubrication of finite journal bearings using Jenkins model. *Lubrication Science*, 29 (7): 1-14.
14. Patel, D.A., & Kataria, R. C. (2022). Combined effect of circumferential roughness and squeeze velocity on ferrofluid squeeze film with rotating sphere and rough plate. *Proceedings of the Institution of Mechanical Engineers Part C: Journal of Mechanical Engineering Science*, 236(24).
15. Shah, R.C., & Patel, D. A. (2016). On the ferrofluid lubricated squeeze film characteristics between a rotating sphere and a radially rough plate. *Meccanica*, 51(8), 1973-1984.
16. Prakash, J., & Tiwari, K. (1982). Lubrication of a porous bearing with surface corrugations. *Journal of Lubrication Technology*, 104, 127-134.
17. Wu, H. (1978). A review of porous squeeze films. *Wear*, 47(2):371-385.
18. Shah, R.C., & Bhat, M.V. (2004). Anisotropic permeable porous facing and slip velocity on squeeze film in an axially undefined journal bearing with ferrofluid lubricant. *Journal of Magnetism and Magnetic Materials*, 279(2–3), 224–230.
19. Patel, J.R., & Deheri, G.M. (2016). Combined effect of slip velocity and roughness on the Jenkins model based Ferrofluid lubrication of a curved rough annular squeeze film. *Journal of Applied fluid Mechanics*, 9(2), 855-865.
20. Chan, D.Y.C., & Horn, R. G. (1985). The drainage of thin liquid films between solid surfaces. *Journal of Chemical Physics*, 83(10), 5311–5324.
21. Matthewson, M. J. (1988). Adhesion of spheres by thin liquid films. *Philosophical Magazine A*, 57(2): 207-216.

22. Lin, J. R. (2000). Squeeze film characteristics between a sphere and a flat plate: couple stress fluid model. *Computers and Structures*, 75, 73-80.
23. Shah, R. C., & Bhat, M.V.(2003). Ferrofluid lubrication of a parallel plate squeeze film bearing. *Theoretical and Applied Mechanics*, 30, 221-240.

Appendix A

$$\frac{\partial}{\partial z} \left(\eta \frac{\partial u}{\partial z} \right) = \frac{1}{\left(1 - \frac{\rho \alpha^2 \bar{\mu} H}{2\eta} \right)} \frac{\partial}{\partial r} \left(p - \frac{1}{2} \mu_0 \bar{\mu} H^2 \right). \quad (\text{A1})$$

Integrating Eq. (A1) twice with respect to z, one obtains

$$\frac{\partial u}{\partial z} = \frac{1}{\eta \left(1 - \frac{\rho \alpha^2 \bar{\mu} H}{2\eta} \right)} \left[\frac{\partial}{\partial r} \left(p - \frac{1}{2} \mu_0 \bar{\mu} H^2 \right) \right] z + A, \quad (\text{A2})$$

$$u = \frac{1}{\eta \left(1 - \frac{\rho \alpha^2 \bar{\mu} H}{2\eta} \right)} \left[\frac{\partial}{\partial r} \left(p - \frac{1}{2} \mu_0 \bar{\mu} H^2 \right) \right] \frac{z^2}{2} + Az + B, \quad (\text{A3})$$

where A and B being constant

of integration.

Using the first condition of Eq. (14) and Eq. (A2), yields $B = \frac{1}{s} \frac{\partial u}{\partial z} \Big|_{z=0}$

Using the second condition of Eq. (14), one obtains from Eq. (A2)

$$A = \frac{-sh^2}{2\eta(1+sh) \left(1 - \frac{\rho \alpha^2 \bar{\mu} H}{2\eta} \right)} \left[\frac{\partial}{\partial r} \left(p - \frac{1}{2} \mu_0 \bar{\mu} H^2 \right) \right]$$

Substituting the above values of A and B in Eq. (A2), yields Eq. (16) of the present research paper.

Appendix B

$$\text{when } \mathbf{M}^* = \frac{1}{2} (\nabla \times \mathbf{q}) \times \mathbf{M} \quad (\text{B1})$$

employing to the Eq. (4) takes the form

$$\rho \left[\frac{\partial \mathbf{q}}{\partial t} + (\mathbf{q} \cdot \nabla) \mathbf{q} \right] = -\nabla p + \eta \nabla^2 \mathbf{q} + \mu_0 (\mathbf{M} \cdot \nabla) \mathbf{H} + \frac{\rho \alpha^2 \nabla}{2} \times \left(\frac{\mathbf{M}}{M} \times \{ (\nabla \times \mathbf{q}) \times \mathbf{M} \} \right) \quad (\text{B2})$$

Put $\mathbf{M} = \bar{\mu} \mathbf{H}$ in Eq. (B2)

1. Last term of Eq. (B2) becomes

$$\frac{\rho \alpha^2 \nabla}{2} \times \left(\frac{\mathbf{M}}{M} \times \{ (\nabla \times \mathbf{q}) \times \mathbf{M} \} \right) = \frac{\rho \alpha^2 \bar{\mu}}{2} \nabla \times \left(\frac{\mathbf{H}}{H} \times \{ (\nabla \times \mathbf{q}) \times \mathbf{H} \} \right) \quad (\text{B3})$$

which modifies the velocity of the fluid. At this point one observes that Neuringer – Rosensweig model modifies the pressure while Jenkins model modifies both the pressure and velocity of the fluid.

2. Second last term of Eq. (B2) becomes

$$\mu_0(\mathbf{M} \cdot \nabla) \mathbf{H} = \mu_0 \bar{\mu} (\mathbf{H} \cdot \nabla) \mathbf{H} \quad (\text{B4})$$

Using vector identity for $(\mathbf{H} \cdot \nabla) \mathbf{H}$ and assuming that the fluid is electrically non-conducting and that the displacement current is negligible so that $\nabla \times \mathbf{H} = \mathbf{0}$, Eq. (B4) becomes

$$\mu_0(\mathbf{M} \cdot \nabla) \mathbf{H} = \frac{1}{2} \mu_0 \bar{\mu} \nabla(H^2) \quad (\text{B5})$$

Using Eq.s (B3) and (B5), Eq. (B2) yields

$$\rho \left[\frac{\partial \mathbf{q}}{\partial t} + (\mathbf{q} \cdot \nabla) \mathbf{q} \right] = -\nabla p + \eta \nabla^2 \mathbf{q} + \frac{1}{2} \mu_0 \bar{\mu} \nabla H^2 + \frac{\rho \alpha^2 \bar{\mu}}{2} \nabla \times \left(\frac{\mathbf{H}}{H} \times \{(\nabla \times \mathbf{q}) \times \mathbf{H}\} \right) \quad (\text{B6})$$

Assuming that the flow is quasi steady, fully developed, axially symmetric and incompressible, the momentum equation for a fluid film reduces to

$$-\rho \frac{v^2}{r} = -\frac{\partial p}{\partial r} + \eta \frac{\partial^2 u}{\partial z^2} + \frac{1}{2} \mu_0 \bar{\mu} \frac{\partial H^2}{\partial r} - \frac{\rho \alpha^2 \bar{\mu} H}{2} \frac{\partial^2 u}{\partial z^2}, \quad \frac{\partial p}{\partial z} = 0 \text{ and } \eta \frac{\partial^2 v}{\partial z^2} = 0 \quad (\text{B7})$$

Solving $\eta \frac{\partial^2 v}{\partial z^2} = 0$ under boundary conditions $v = 0$ when $z = 0$ and $z = h$

We get, velocity component $v = 0$

$$\text{Put } v = 0 \text{ in Eq. (B7), one obtains } 0 = -\frac{\partial p}{\partial r} + \eta \frac{\partial^2 u}{\partial z^2} + \frac{1}{2} \mu_0 \bar{\mu} \frac{\partial H^2}{\partial r} - \frac{\rho \alpha^2 \bar{\mu} H}{2} \frac{\partial^2 u}{\partial z^2}$$

which represent Eq. (13) of the present study.

Appendix C

Calculation of maximum magnetic field strength and K

From Eq. (3), $H^2 = \frac{Kr^2(a-r)}{a}$, which is maximum at $r = 2a/3$ giving

$$H_{Max}^2 = 0.148 \times 10^{-4} K \text{ for } a=0.01,$$

for $K = \frac{10^9}{1.48}$, $H \approx O(10^2)$ or $O(H) \approx 2$.

where O indicates the order.